Natural genetic variation underlying the negative effect of elevated CO_2 on ionome composition in *Arabidopsis thaliana*

Océane Cassan[1], Léa-Lou Pimparé[1], Timothy Mozzanino[1], Cécile Fizames[1], Sébastien Devidal[2], Fabrice Roux[3], Alexandru Milcu[2,4], Sophie Lèbre[5], Alain Gojon[1], Antoine Martin[1*]

[1] IPSiM, Univ Montpellier, CNRS, INRAE, Institut Agro, 34060, Montpellier, France

[2] Montpellier European Ecotron, Univ Montpellier, CNRS, Campus Baillarguet, 34980, Montferrier-sur-Lez, France

[3] Laboratoire des Interactions Plantes-Microbes-Environnement, Institut National de Recherche pour l'Agriculture, l'Alimentation et l'Environnement, CNRS, Université de Toulouse, Castanet-Tolosan, France

[4] CEFE, Univ Montpellier, CNRS, EPHE, IRD, 34293, Montpellier, France

[5] IMAG, Univ Montpellier, CNRS, Montpellier, France

*Author for correspondence: antoine.martin@cnrs.fr

Abstract

The elevation of atmospheric CO_2 leads to a decline in the plant mineral content, which might pose a significant threat to food security in the coming decades. To date, very few genes have been identified as having a role in the negative effect of elevated CO_2 on plant mineral composition. Yet, several studies have shown a certain degree of diversity in the ionome's response to elevated CO_2, associated with genotypic variation. This suggests the existence of genetic factors controlling the effect of CO_2 on ionome composition. However, no large-scale studies have been carried out to date to explore the genetic diversity of the ionome responses to elevated CO_2. Here, we used six hundred *Arabidopsis thaliana* accessions, representing geographical distributions ranging from worldwide to regional and local environments, to analyze the natural genetic variation underlying the negative effect of elevated CO_2 on the ionome composition in plants. We show that the growth under elevated CO_2 leads to a global and important decrease of the ionome content whatever the geographic distribution of the population. We also observed a high range of genetic diversity in the response of the ionome composition to elevated CO_2, and we identified sub-populations, showing effects on their ionome ranging from the most pronounced to resilience or even to a benefit in response to elevated CO_2. Using genome-wide association mapping on the response of each mineral element to elevated CO_2 or on integrative traits, we identified a large set of QTLs and genes associated with the ionome response to elevated CO_2. Finally, we demonstrate that the function of one of these genes is associated to the negative effect of elevated CO_2 on the plant mineral composition. This resource will contribute to understand the genetic mechanisms underlying the negative effect of elevated CO_2 on plant mineral nutrition, and could help towards the development of crops adapted to a high-CO_2 world.

24 **Introduction**

25 The elevation of atmospheric CO_2 concentration leads to a decline in the mineral composition
26 of C3 plants (Gojon et al., 2023). The negative effect of elevated CO_2 on plant mineral
27 composition has been observed worldwide, and alters the content of nutrients that are
28 essential for human nutrition, such as nitrogen (N) and proteins, iron (Fe) or zinc (Zn) (Loladze,
29 2014). Therefore, the rise in atmospheric CO_2 poses a significant threat to food security in the
30 coming decades. Indeed, several modeling approaches predict a decrease in plant-based
31 nutrient availability due to the negative effect of elevated CO_2 on the mineral status of plants,
32 leading to an additional risk of nutritional deficiency for hundreds of millions of people (Medek
33 et al., 2017; Ebi and Loladze, 2019). However, the reasons why elevated CO_2 leads to the
34 degradation of plant mineral composition are far from being well understood. To date, only a
35 few genes with a potential regulatory role on this effect have been identified (Gao et al., 2019;
36 Umnajkitikorn et al., 2020; Yang et al., 2020; Bouain et al., 2022; Sun et al., 2022; Cassan et
37 al., 2023). Despite their limited number, these studies show that the detrimental effect of high
38 CO_2 on the plant mineral status has genetic bases. In addition to this, several reports suggest
39 that exploring the natural genetic variability of plants represents a major opportunity to
40 understand the mechanisms by which high CO_2 leads to a decline in plant mineral composition
41 (Myers et al., 2014; Zhu et al., 2018; Marcos-Barbero et al., 2021). Indeed, a significant
42 diversity in the response of mineral composition to high CO_2 has been observed in several
43 plant species. For protein and therefore N content, as well as for Fe or Zn content, substantial
44 variations have been observed between small panels of genotypes from different species
45 (Myers et al., 2014; Zhu et al., 2018; Marcos-Barbero et al., 2021). This implies the presence
46 of a genetic diversity reservoir, which can facilitate the understanding of the ionome's
47 response to high CO_2 and subsequently provide an opportunity to alleviate this negative

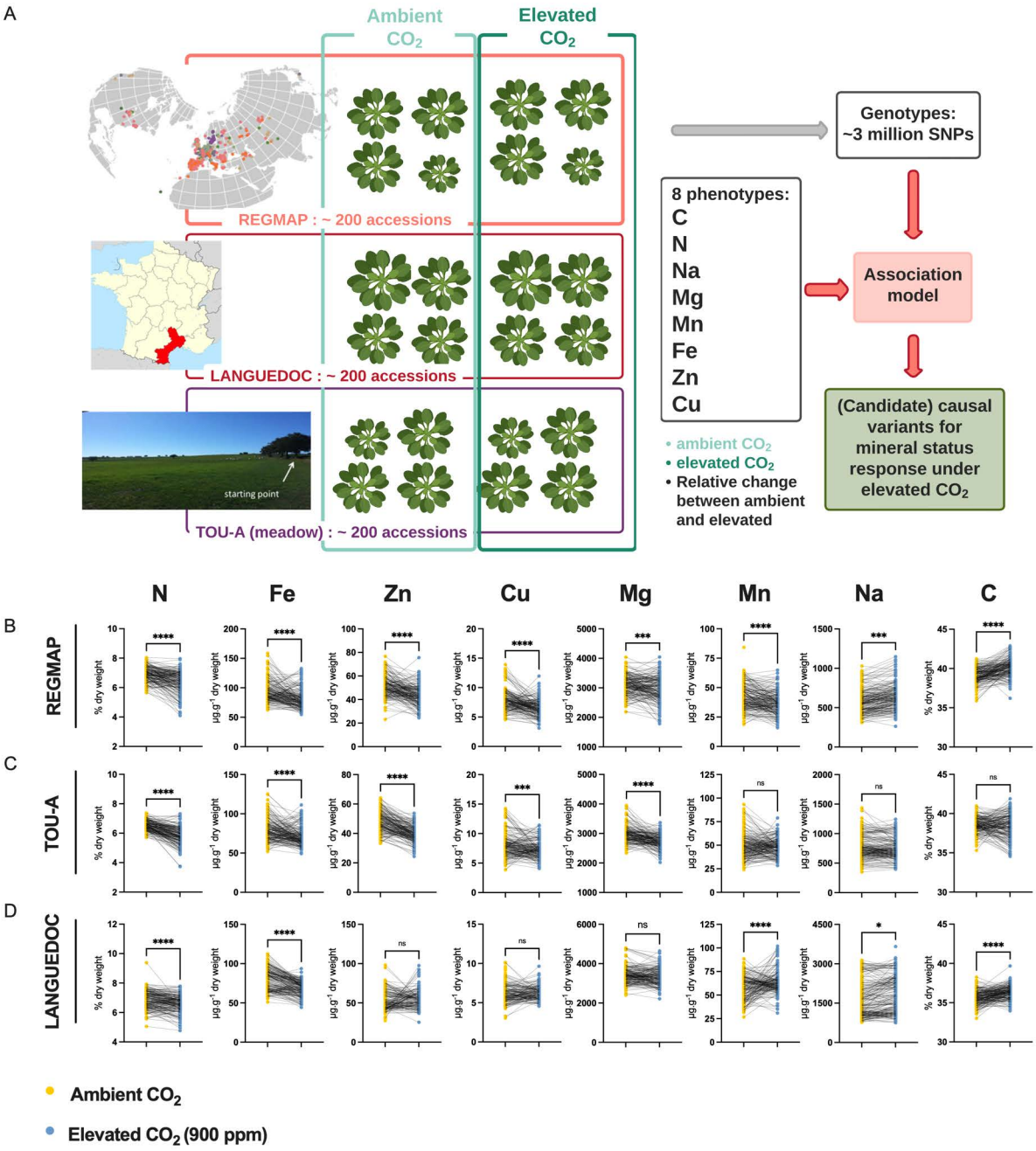

Figure 1: Elevated CO_2 negatively impacts the ionome content at the population-scale level in *Arabidopsis thaliana*. A. Representation of the experimental design used in this study. The content of eight mineral elements was assessed for around 600 *Arabidopsis thaliana* accessions coming from the REGMAP (B), LANGUEDOC (C) and TOU-A (D) populations. Each dot represents the value of the content of a mineral element for one accession (yellow: ambient CO_2 (aCO_2, ~420 ppm), blue: elevated CO_2 (eCO_2, 900 ppm). N (% of dry weight), Fe ($\mu g.g^{-1}$ dry weight), Zn ($\mu g.g^{-1}$ dry weight), Cu ($\mu g.g^{-1}$ dry weight), Mg ($\mu g.g^{-1}$ dry weight), Mn ($\mu g.g^{-1}$ dry weight), Na ($\mu g.g^{-1}$ dry weight), C (% of dry weight). Asterisks indicate significant differences (Paired Wilcoxson test; *, $P<0.05$; **, $P<0.005$; ***, $P<0.0005$). ns; not significant.

48 impact. However, in order to identify the genetic determinants of this negative response of
49 the ionome to high CO_2, large-scale approaches are necessary, but are still lacking for the
50 moment. The objective of this work was to fill the aforementioned knowledge gap by using a
51 large collection of natural genotypes of the model plant *Arabidopsis thaliana.* This allowed to
52 explore in depth the natural variation of the ionome response to elevated CO_2, and to
53 generate a resource of phenotypic data that can be used in association genetics approaches.
54 To this end, we used several hundreds of accessions from different geographic scales of *A.*
55 *thaliana*, and analyzed their leaf mineral composition under contrasted conditions of CO_2
56 concentration. This allowed us to extract the general trends in the leaf ionome response to
57 high CO_2, and to identify a large set of genes associated with the variation in the mineral
58 composition of plants in response to high CO_2. By combining this information with genome
59 expression data under elevated CO_2, we end up by functionally validating one of these genes
60 for its importance in the reduction of Zn content under elevated CO_2. Our results open the
61 way for a better understanding of the genetic and molecular mechanisms involved in the
62 regulation of plant mineral nutrition by the elevation of atmospheric CO_2.
63
64 **Results**
65 In order to explore the natural variation and identify its underlying genetic basis associated
66 with the negative effect of elevated CO_2 on plant ionome, we used three populations of *A.*
67 *thaliana* representing different geographic scales (i.e., the worldwide REGMAP population,
68 the LANGUEDOC regional population and the local TOU-A population from east of France) and
69 displaying different levels of genetic diversity (Fig. 1A). These populations were grown under
70 ambient or elevated CO_2, and we measured in each accession the composition of their ionome
71 in rosettes, including C, N, Na, Fe, Mg, Mn, Zn and Cu content.

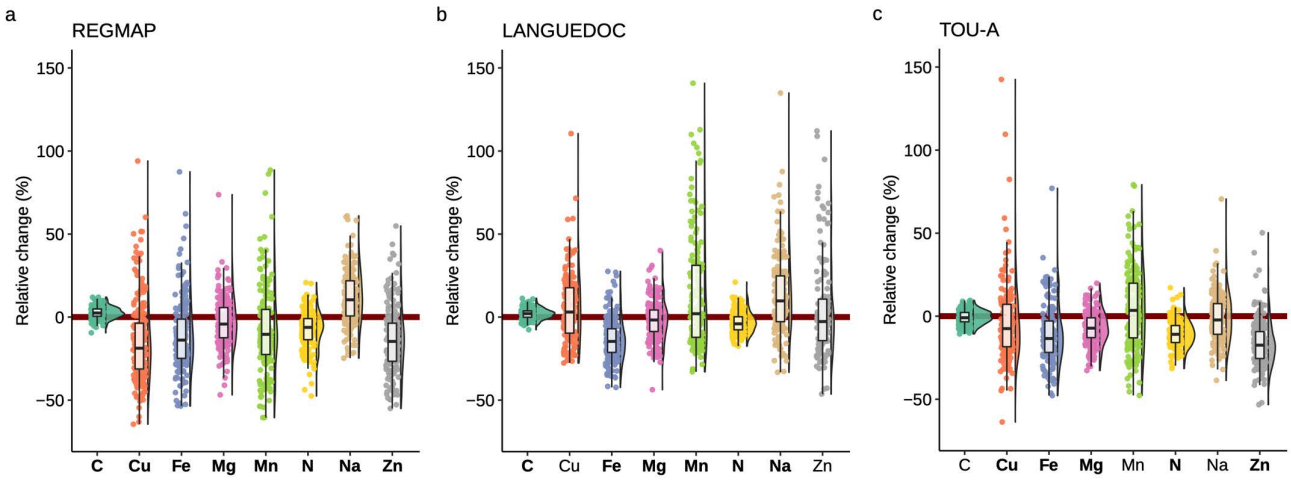

Figure 2: Elevated CO_2 leads to high phenotypic diversity of ionome response in *Arabidopsis thaliana*. Distributions of the relative change (%) of the content of 8 mineral elements between elevated CO_2 and ambient CO_2, in each population (A: REGMAP, B: LANGUEDOC, C: TOU-A). Each dot represents the value of the relative change of the content a mineral element for one accession. The name of the element appears in bold if the mean of the element in elevated CO_2 is significantly different from the mean of the element in ambient CO_2 (Paired wilcoxon test, significance threshold of 0.05).

72 **Elevated CO_2 globally decreases ionome content at the population level, whatever the**
73 **geographic scale.**
74 In the three *A. thaliana* populations, we observed a global and important decrease of the
75 ionome content when plants were grown under elevated CO_2 as compared to ambient CO_2.
76 This was particularly the case for N and Fe, for which the decrease in content was very robust
77 and important in each of the population analyzed (Fig. 1B-D). Zn, Cu and Mg content were also
78 negatively affected to a significant extent by the growth under elevated CO_2 in the REGMAP
79 and in the TOU-A populations (Fig. 1B, C), although not significantly in the LANGUEDOC
80 population (Fig. 1D). More variability for the effect of elevated CO_2 was observed on Mn and
81 Na content, which were decreased in the REGMAP population, but not significantly changed
82 in the TOU-A and LANGUEDOC populations, respectively. In parallel, the C content of these
83 populations increased under elevated CO_2, by very significant factors for the REGMAP and the
84 LANGUEDOC populations. Altogether, these observations demonstrate that elevated CO_2 has
85 on average a negative impact on the mineral content of natural genotypes of *A. thaliana* at
86 the population-scale, whatever their geographic distribution.
87
88 **The ionome of *Arabidopsis thaliana* natural accessions displays a high range of phenotypic**
89 **diversity in response to elevated CO_2.**
90 To explore the effect of elevated CO_2 in each accession, we calculated the relative change in
91 nutrient composition of *A. thaliana* accessions from the three populations in response to
92 elevated CO_2. In agreement with the results previously mentioned, we observed that the
93 median relative change of most nutrient content at the population-level was negatively
94 affected by elevated CO_2 (Fig. 2). But the most striking observation was the genetic diversity
95 of ionome response observed in these populations. Indeed, while most the natural accessions

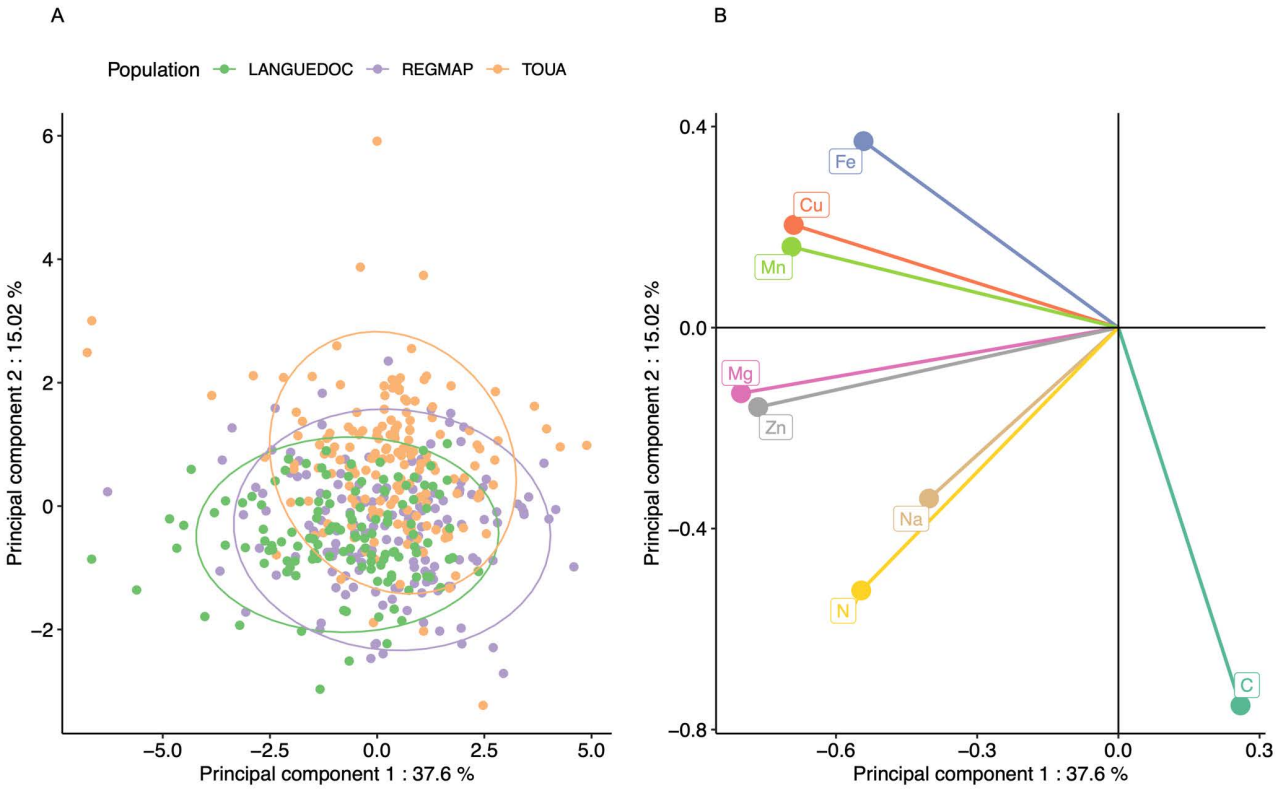

Figure 3: Elevated CO_2 results in a general pattern of ionome variation common to most accessions constituting natural populations of *Arabidopsis thaliana*. Principal Component Analysis (PCA) was performed using the variation of each element in response to elevated CO_2. A. Natural accessions were positioned on the PCA and colored based on population. B. Contribution of each element to the PCA axis.

96 were negatively affected by elevated CO_2 (with a negative relative ratio of their nutrient
97 content between ambient and elevated CO_2), a considerable number of accessions were
98 rather not affected by elevated CO_2, or even positively affected, therefore showing an
99 improved nutrient composition under elevated CO_2. For macronutrients like N, the relative
100 change of concentration between ambient and elevated CO_2 varied from 20% to -50%, and for
101 micronutrients like Cu, Fe or Zn, the relative change of concentration between ambient and
102 elevated CO_2 varied from 100% to -60% (Fig. 2). In addition, some differences among nutrients
103 were observed between populations. For instance, a smaller dispersion of Fe relative change
104 in the LANGUEDOC population, against a higher distribution of Mn relative change.
105 In order to explore the behavior of the different elements in response to elevated CO_2 and to
106 observe the structure of phenotypic variation, we performed a principal component analysis
107 (PCA) of the relative change in the 8 elements for the accessions from the three populations.
108 The accessions from all populations seem to have globally similar responses to elevated CO_2,
109 as suggested by the overlap of the three populations in the two first principal components
110 (Fig. 3A). The first component of the PCA described a clear antagonistic trend between C
111 content and the change of other mineral elements (Fig. 3B), suggesting that most of the
112 variation between accessions in term of mineral response (almost 40%) could be driven by
113 one or a few mechanisms resulting in an inverse variation between the whole ionome and C
114 change (Fig. 3B). Interestingly, the second component, explaining almost 15% of the variation
115 among accessions in term of mineral response, was mainly driven jointly by change in N and
116 C concentration. Altogether, these results show that there is a marked and large variability
117 among accessions in their mineral concentration in response to elevated CO_2, illustrated by
118 accessions negatively affected by elevated CO_2 and others positively affected by elevated CO_2.

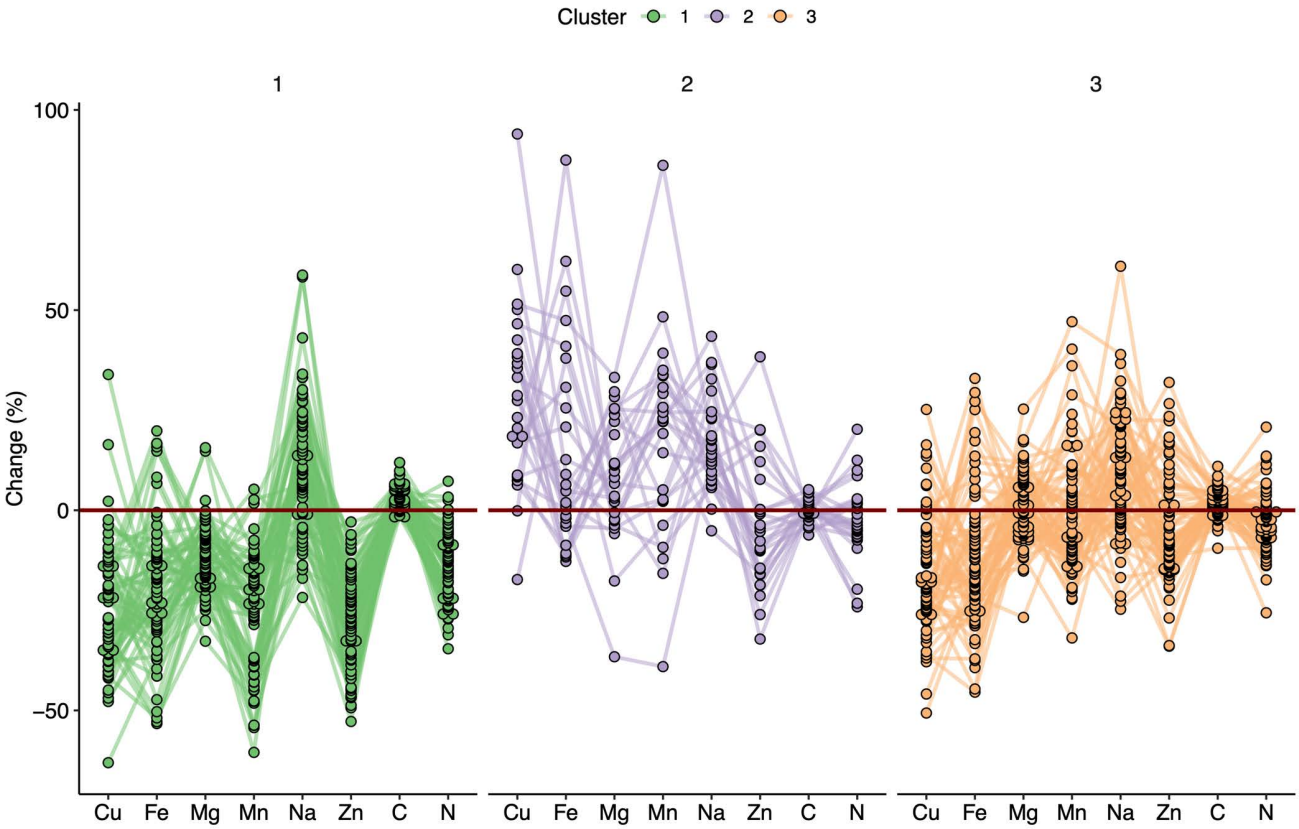

Figure 4: Variation in the response of the ionome to elevated CO_2 identifies contrasting subpopulations inside the REGMAP panel. K-means clustering was performed in the REGMAP accessions to identify different subpopulations. Each accession is represented by a dot, connected by a line between each element. Cluster 1:65 accessions. Cluster 2: 25 accessions. Cluster 3: 69 accessions.

119 In order to explore specific behavior of sub-populations, we clustered the accessions from the
120 REGMAP panel via a k-means approach. This multivariate clustering resulted in the
121 partitioning of accessions in three groups (Fig.4 – Suppl. Table 1). Cluster 1 displayed the most
122 negative pattern of ionome response to elevated CO_2. Inversely, accessions included in Cluster
123 2 displayed a globally positive response, with the highest relative change for almost all mineral
124 elements, except for C content. These accessions did not appear to be clustered
125 geographically with respect to their collection origin in the REGMAP panel (Suppl. Fig. 1),
126 which is in line with the high genetic diversity of response to elevated CO_2 observed at smaller
127 geographical scales (Fig.2). Finally, Cluster 3 displayed a resilient pattern, with accessions
128 showing a globally attenuated response to elevated CO_2. Interestingly, the large phenotypic
129 diversity of the ionome observed in the three populations in response to high CO_2, as well as
130 the presence of contrasted subpopulations in the REGMAP panel, suggests the presence of
131 genetic determinants associated with this response.
132
133 **Genetic architecture of the ionome response to elevated CO_2, and identification of genetic**
134 **determinants**
135 We ran Genome-Wide Association (GWA) mapping to describe the genetic architecture of the
136 ionome response to elevated CO_2, and to fine-map candidate genes underlying the detected
137 quantitative trait loci (QTLs). We focused here on the phenotypic data collected on the
138 REGMAP population, and used the sequencing data available for this population (Arouisse et
139 al., 2020). We included in this analysis the level of each mineral under ambient and under
140 elevated CO_2, as well as the relative change between ambient and elevated CO_2 for each
141 element. We also included a trait corresponding for each accession to the coordinate on the
142 first and on the second PCA axes (PCA1 and PCA2) explaining collectively more than 50% of

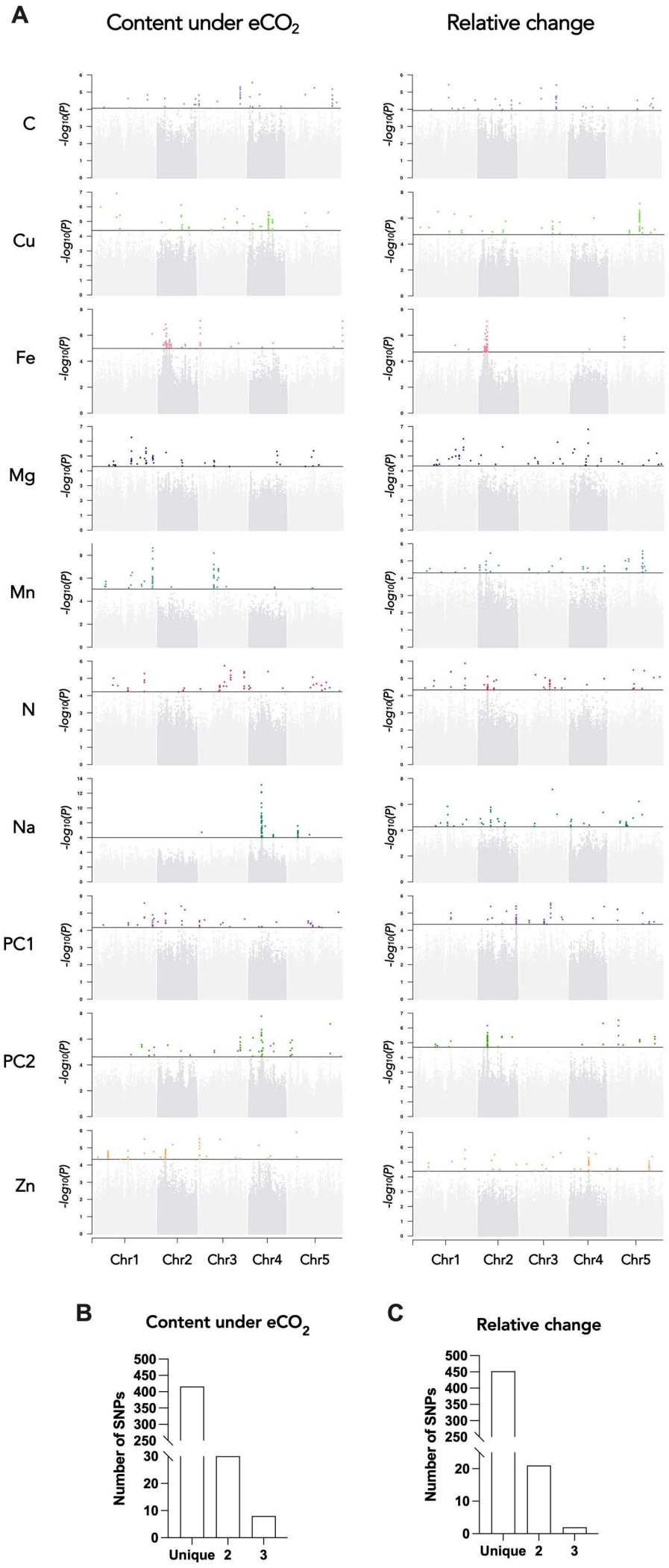
A
Content under eCO2
Relative change
C
Cu
Fe
Mg
Mn
N
Na
PC1
PC2
Zn
-log10(P)
Chr1
Chr2
Chr3
Chr4
Chr5
B
Content under eCO2
Number of SNPs
Unique
2
3
C
Relative change
Number of SNPs
Unique
2
3

Figure 5: Genetic architecture of the response of the ionome to elevated CO_2 in the REGMAP panel of *Arabidopsis thaliana*. A. Manhattan plots for the content of eight mineral elements under elevated CO_2, or for the relative change of the content of mineral elements between elevated CO_2 and ambient CO_2. For each Manhattan plot, SNPs with the 50 most significant P-value, located above the horizontal line, are colored. Bar plots showing the number of SNPs identified by GWAs for traits under elevated CO_2 (B) or for the relative change of the content of mineral elements between elevated CO_2 and ambient CO_2 (C) that are unique to one element or shared between 2 or 3 traits.

143 ionomic variation (Fig. 3). Therefore, these values correspond to traits driving and
144 summarizing a large part of the ionome variation under elevated CO_2. This resulted as a whole
145 in running GWA mapping on 30 different single-trait GWAS. The overall approach was first
146 validated by observing expected results for traits phenotyped under ambient CO_2. For
147 instance, we observed a very strong peak for the Na content at the locus of the *HKT1* gene
148 (Suppl. Fig. 2A), which is known to be involved in the natural genetic variation of Na content
149 in *Arabidopsis thaliana* (Baxter et al., 2010), or a strong peak for the N content at the locus of
150 the *NIA1* gene (Suppl. Fig. 2B), encoding for an isoform of the nitrate reductase required for
151 the first step of nitrate reduction and associated with natural genetic variation of N content
152 in *A. thaliana* (North et al., 2009).
153 GWA mapping revealed a polygenic architecture for each phenotypic trait, although its
154 complexity largely differs among traits. For instance, very few and neat peaks of association
155 were detected Na and Mn content under elevated CO2, or of Fe and Cu relative change
156 between ambient and elevated CO_2 (Fig.5A, Suppl. Fig. 3). On the other hand, a more complex
157 genetic architecture with the detection of a large number of QTLs was observed for traits
158 related to N or C content (Fig.5A, Suppl. Fig. 3). For each of the traits that have been analyzed
159 under elevated CO_2 or corresponding to the relative change of their content between ambient
160 and elevated CO_2, we isolated the 50 SNPs with the most significant p-value, hereafter named
161 top SNPs (Fig. 5A, Suppl. Tables 2 and 3). In order to identify the overlap between the genetic
162 architecture of each trait, we looked whether some of the top SNPs were shared among traits.
163 While the large majority of SNPs were specific to one trait, 30 and 21 SNPs were shared
164 between two traits for the content under elevated CO_2 or for the relative change between
165 ambient and elevated CO_2, respectively (Fig. 5B and C, Supplemental Tables 2 and 3). In
166 addition, 8 and 2 SNPs were shared between three traits for the content under elevated CO_2

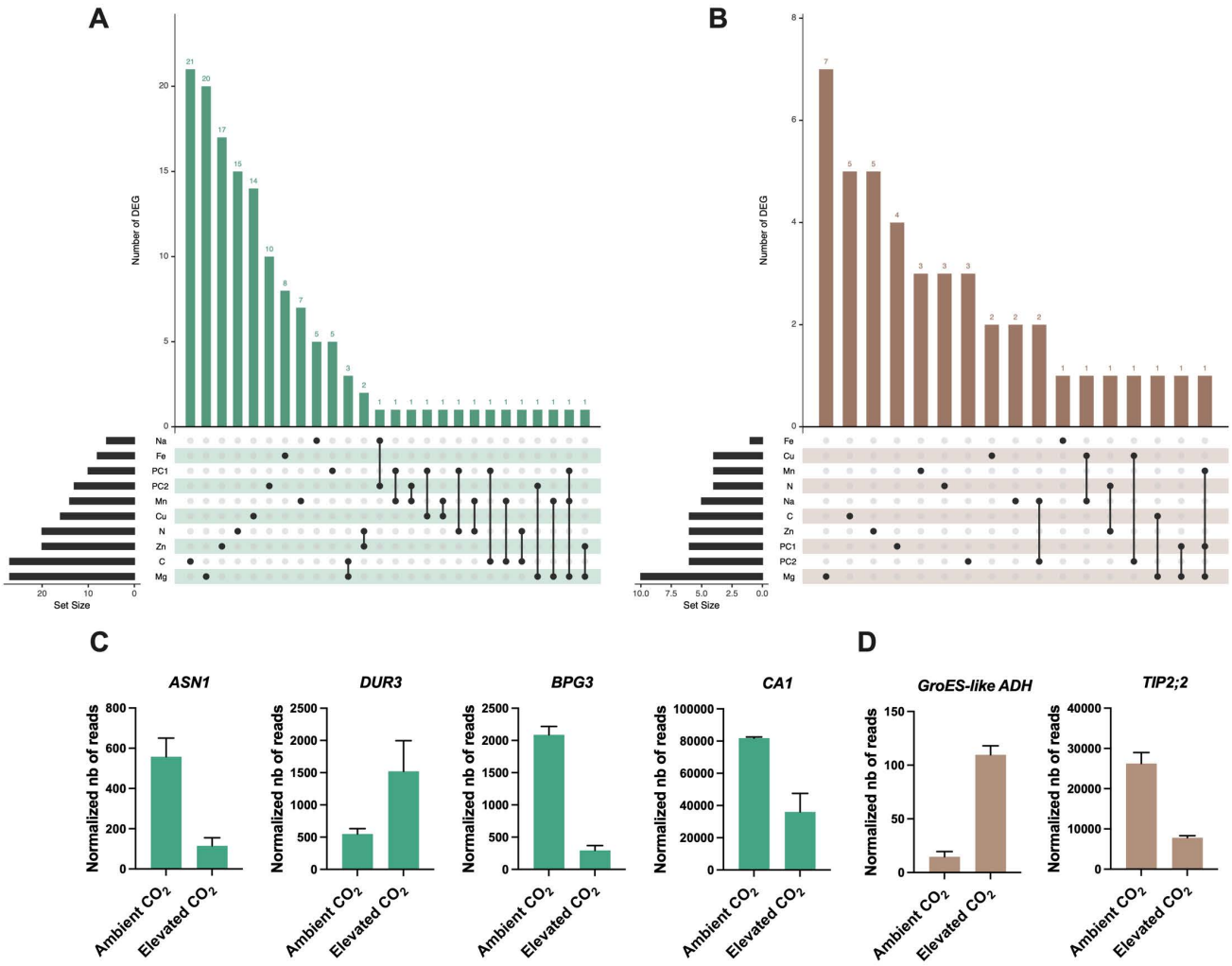

Figure 6: Identification of genes detected by GWA mapping and differentially regulated by elevated CO_2. Intersection between elevated CO_2-DEG in shoot (A) or root (B) and genes identified by GWA mapping. UpSet plots display the number of elevated CO_2-DEG that are associated to a locus identified for the content or the relative change of one or several mineral elements under elevated CO_2. Illustration of the pattern of elevated CO_2-DEG in shoot (C) or root (D) also identified by GWA mapping.

167 or for the relative change between ambient and elevated CO_2, respectively (Fig. 5B and C,
168 Supplemental Tables 2 and 3). Most of the shared SNPs were associated with micronutrients
169 (Fe, Mn, Zn and Mg content) and with N and/or with the first component of the PCA axis. An
170 interesting QTL located on chromosome 1 was notably associated with 6 traits, displaying
171 SNPs shared between Mn, Zn and N relative change and SNPs shared between Mn, N and PC1
172 content under elevated CO_2 (Fig. 5A, Suppl. Tables 2 and 3). Another QTL located on
173 chromosome 3 encompasses SNPs shared between Fe, Zn and PC1 content under elevated
174 CO_2 (Fig. 5A, Suppl. Table 2).
175 We next identified for each trait a list of the genes located at ±25 kb from the top 50 SNPs,
176 which corresponds to the rough estimate of the decay of linkage disequilibrium identified in
177 *A. thaliana* at the worldwide scale (Kim et al., 2007). This resulted in a list of genes for each
178 element, ranging from 154 to 422 genes depending on the element (Suppl. Tables 2 and 3).
179 Among others, several genes associated with top 50 SNPs were identified as obvious
180 candidates of the effect of elevated CO_2 on plant nutrition and ionome content. This was the
181 case of *ZINC INDUCED FACILITATOR 1* (*ZIF1*, *AT5G13740*) and *ZIF-LIKE1* (*AT5G13750*), linked
182 with SNPs identified for Zn content under elevated CO_2, and involved Zn sequestration
183 mechanisms (Lee et al., 2021). We also noticed the link between SNPs identified for Zn relative
184 change and *TIP2;2* (*AT4G17340*), known to be involved in Zn root-to-shoot translocation
185 (Wang et al., 2022). Concerning N relative change, some of the top 50 SNPs were linked to
186 *ASN1* (*AT3G47340*), which is an actor of N status and remobilization (Lam et al., 2003;
187 Gaufichon et al., 2017). Some of the top 50 SNPs identified for Fe relative change were linked
188 to *MCO2* (*AT5G21100*) and *MCO3* (*AT5G21105*) genes, which have been recently
189 characterized as actors of the regulation of Fe homeostasis (Brun et al., 2022). Finally, it is
190 interesting to note that the QTL located on chromosome 3 mentioned above displaying

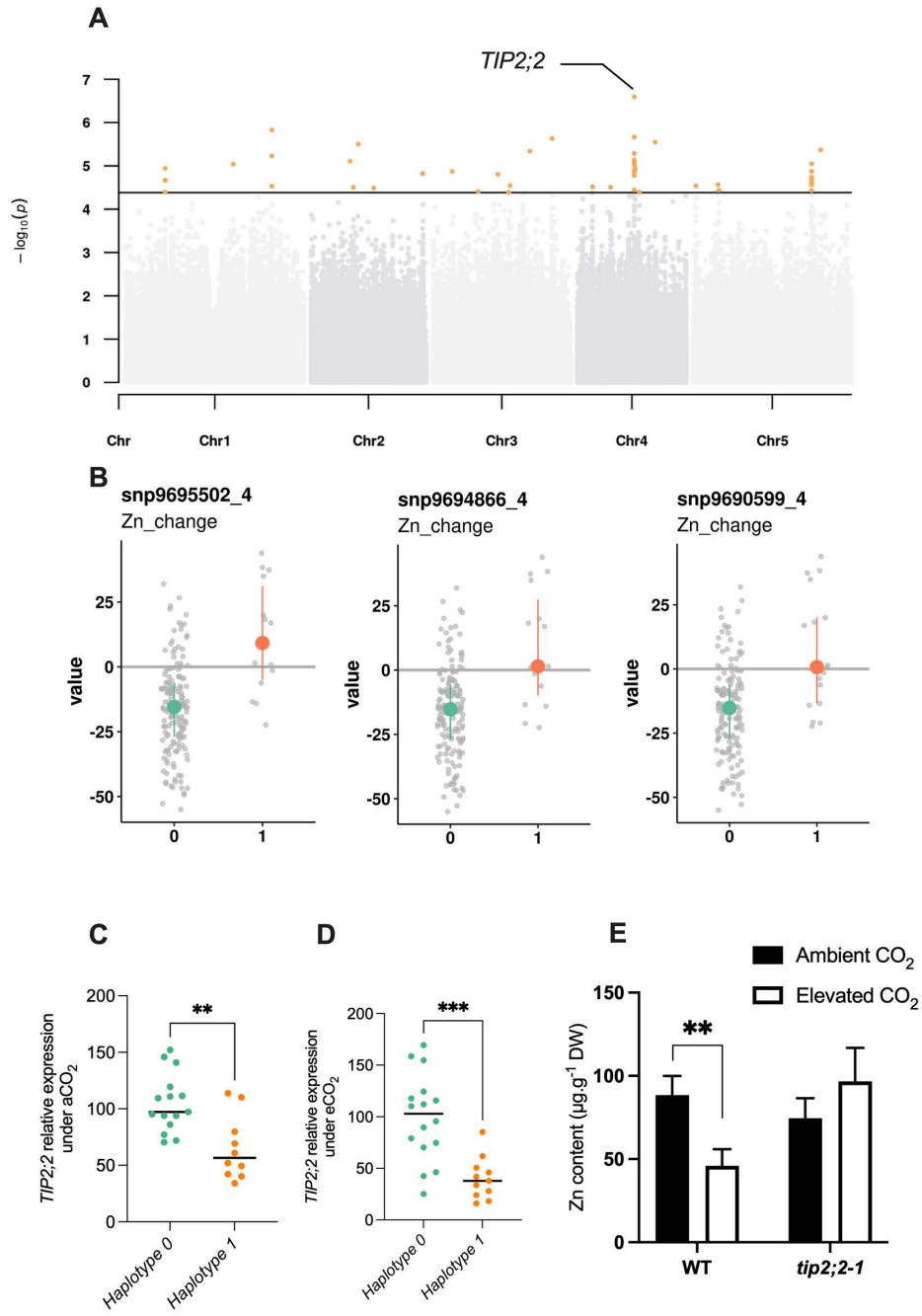

Figure 7: Natural variation of the *TIP2;2* gene is associated with improved responses of Zn content to elevated CO_2. A. Manhattan plot of the relative change of Zn content between elevated CO_2 and ambient CO_2 showing the presence of a peak closed to the *TIP2;2* locus. **B.** Comparison of haplotypes and their relative change of Zn content between elevated CO_2 and ambient CO_2. Three SNPs located at the *TIP2;2* locus are associated to an improvement of Zn content under elevated CO_2 for accessions that possess them (haplotype 1) compared to the rest of the population (haplotype 0). **C, D.** Relative expression of *TIP2;2* in the roots under ambient (**C**) or elevated (**D**) CO_2 for accessions belonging to haplotype 0 or haplotype 1. Relative expression levels were calculated based on *UBQ10* as internal control. Horizontal black line represented the median of each group of haplotypes. ***P < 0,001, **P < 0,01, unpaired Mann-Whitney test. **E.** Shoot Zn content under ambient or elevated CO_2 for WT (Columbia) and *tip2;2-1* mutant. Data are presented as the mean (with SD) of 5 and 6 biological repeats for the WT and *tip2;2-1*, respectively. **P < 0.01, unpaired Mann-Whitney test.

191 significant shared SNPs identified for Fe, Zn and PC1 content under elevated CO_2 was
192 associated among other genes with *ISU2* (*AT3G01020*), coding for one of the Fe-S clusters in
193 *Arabidopsis thaliana*, which are known to be essential for photosynthesis and metabolism
194 (Balk and Schaedler, 2014). Altogether, this demonstrated that genes identified through this
195 approach represent a large and valuable reservoir of candidates to study and to counteract
196 the effect of elevated CO_2 on plant nutrition and ionome content.
197 To analyze how these genes identified by GWA mapping are regulated by elevated CO_2, we
198 performed RNA-seq from shoots and roots grown under ambient and elevated CO_2.
199 Differentially expressed genes (DEG) associated to the effect of elevated CO_2 were identified
200 from shoots and roots (Suppl. Table 4). We compared the list of shoots or roots elevated CO_2-
201 DEG with the list of genes identified by GWA mapping for each element, which resulted in a
202 list of 182 genes identified by GWA mapping and differentially regulated by elevated CO_2 in
203 shoot or in roots (Suppl. Table 5), making them relevant candidates to be involved in the
204 response of the mineral composition of plants to elevated CO_2. Most of these genes were
205 deregulated by elevated CO_2 in shoot (Fig. 6A, B). In shoot or in roots, these genes mainly
206 showed an association with C-, Mg- or Zn-related traits (Fig. 6A, B). Several of these genes,
207 identified by GWA mapping and whose expression is deregulated in response to high CO_2,
208 were known for their role in nutrient homeostasis. This was the case for the *ASN1* and *DUR3*
209 genes, encoding an asparagine synthase and a urea transporter involved in N metabolism and
210 remobilization, both associated here with a N-related peak of association, and whose
211 expression is modulated by high CO_2 in leaves (Fig. 6C). We also observed in the leaves an
212 interesting profile for several genes related to C metabolism and photosynthesis. This was the
213 case for the *BGP3* gene, involved in chloroplast development, or for the carbonic anhydrase
214 *CA1*, both showing a decreased expression in response to high CO_2 and both associated with

215 a peak in C-related GWA mapping under elevated CO_2 (Fig. 6C). In roots, the gene most
216 deregulated in response to high CO_2 was *AT1G64710*, encoding a GroES-type alcohol
217 dehydrogenase, which interestingly is also deregulated in leaves (Fig. 6D). We also observed
218 in the roots that the expression of the *TIP2;2* gene, associated here with a peak detected for
219 Zn relative change GWA mapping, was deregulated in response to elevated CO_2 (Fig. 6D).
220 To go further, we selected one of the association peaks identified by GWA mapping, and
221 sought to functionally validate the importance of this QTL in response to elevated CO_2, in order
222 to demonstrate the value of our data set and GWA mapping analyses. To do so, we selected
223 an association peak located on chromosome 4 and associated with Zn relative change (Fig.
224 7A). More precisely, this association peak displayed the SNPs with the most significant *p*-
225 values and more largely three SNPs that fell into the top 10 SNPs of the trait corresponding to
226 the Zn relative change between ambient and elevated CO_2. The SNPs corresponding to the
227 alternative alleles were associated to an increase of Zn content under elevated CO_2 (Fig. 7B).
228 These SNPs are located very close to the *TIP2;2* (*AT4G17340*) gene, which has been recently
229 characterized as an actor of Zn root-to-shoot translocation (Wang et al., 2022). We thus
230 selected a set of accessions from haplotype 0 (reduced Zn content under elevated CO_2) or
231 haplotype 1 (increased Zn content under elevated CO_2), and analyzed *TIP2;2* expression in the
232 roots under ambient and elevated CO_2. This analysis revealed a haplotype-specific difference
233 in *TIP2;2* expression: under ambient and elevated CO_2, accessions from haplotype 1
234 (correlated with a higher Zn content in the shoot (Fig. 7B)) show a reduced *TIP2;2* expression
235 in the roots compared to those from haplotype 1 (Fig. 7C & D), with a reduction being more
236 pronounced under elevated CO_2. To test the effect of *TIP2;2* expression of Zn content under
237 elevated CO_2, we used the *tip2;2-1* knock-out mutant and compared its Zn content under
238 ambient and elevated CO_2 to this of the WT. We observed that the *tip2;2-1* mutant line did

239 not present any decrease in Zn shoot content in response to elevated CO_2, in opposition to
240 what is observed for the WT (Fig. 7E). In the *tip2;2-1* mutant, Zn content under elevated CO_2
241 was even slightly higher than under ambient CO_2. Altogether, these results demonstrated that
242 these data sets generated in this study and the associated analyses are a valuable resource to
243 identify genes and associated mechanisms involved in the effect of elevated CO_2 on the
244 mineral composition of plants.
245

246 **Discussion**

247 **The natural variation of ionome response to elevated CO_2 in *Arabidopsis thaliana* displays a**
248 **high degree of genetic variation**

249 In the present work, we analyzed the diversity of leaf ionome response to elevated CO_2
250 present in the natural variation of *Arabidopsis thaliana*. In agreement with several other
251 phenotypic traits related to phenology and disease resistance (Brachi et al., 2013; Huard-
252 Chauveau et al., 2013; Roux and Frachon, 2022), we observed a wide range of responses at
253 complementary geographical scales, from accessions with an ionome negatively affected by
254 high CO_2 to accessions with an ionome benefiting from high CO_2. This confirms for the first
255 time on large and complementary sets of natural genotypes what has been observed by meta-
256 analysis on isolated groups of plants worldwide (Loladze, 2014; Myers et al., 2014). The global
257 analysis of the distribution of each mineral element studied suggests firstly a trend where the
258 whole ionome would evolve in a unified manner in response to high CO_2, and in an opposite
259 manner to C. This is in line with a number of studies that have proposed that the accumulation
260 of carbohydrates due to the stimulation of photosynthesis by high CO_2 would be the cause of
261 the decrease in plant mineral composition (Ainsworth and Long, 2005; Thompson et al., 2017;
262 Dusenge et al., 2019; Tausz-Posch et al., 2020). However, the reading of the genetic

263 architecture performed here by a genome-wide association genetics approach suggests that
264 the majority of the genetic mechanisms underlying the negative effect of elevated CO_2 on the
265 ionome are specific to each mineral element. Some specific cases, such as the QTL detected
266 on chromosome 1 and associated with the natural genetic variation of 6 traits among the 20
267 considered, will certainly deserve a more in-depth analysis.
268 By clustering globally distributed accessions according to their ionome sensitivity to high CO_2,
269 we were able to observe that the geographic origin of the accessions likely did not determine
270 their response to CO_2. This suggests that inherent genetic factors, more than those due to
271 local adaption, direct the response of plants to elevated CO_2. This seems consistent since the
272 CO_2 elevation applied here to natural *Arabidopsis thaliana* variants does not correspond to
273 any environment experienced by plants yet, at least for several tens of millions of years
274 (Pearson and Palmer, 2000; Luthi et al., 2008). In this context of brutal and highly impactful
275 environmental change, the presence of cryptic genetic variation often explains the
276 appearance of relatively rapid adaptive mechanisms (Pauls et al., 2013; Cortés and López-
277 Hernández, 2021). Although not formally tested here, it would be interesting to examine
278 whether the variation in the ionome in response to elevated CO_2 shows evidence of cryptic
279 variation. In any case, the presence of high phenotypic diversity in these natural populations
280 of *A. thaliana* demonstrates very clearly the possibility of taking advantage of this genetic
281 variation to understand and alleviate the negative response of plant mineral composition to
282 high CO_2.
283 **GWA mapping of ionome variation under elevated CO_2 identified a large number of genes**
284 **to understand and mitigate the negative effect of high CO_2 on plant mineral composition**
285 In order to understand the genetic mechanisms underlying the effect of high CO_2 on plant
286 mineral composition, and to enable future breeding approaches, we adopted an association

287 genetics approach. This led to the identification of a large number of candidate genes
288 associated to the variation of nutrients under elevated CO_2. Several genes in this list can easily
289 attract attention. In particular, we can note the identification of *ASN1* and *DUR3* genes in two
290 of the loci associated with N content variation under elevated CO_2. *ASN1*, and to a lesser
291 extent *DUR3*, play an important role in the remobilization and the reallocation of N within the
292 plant, and their manipulation can lead to variation in N use efficiency (Lam et al., 2003; Bohner
293 et al., 2015; Gaufichon et al., 2017). This is interesting because for the moment, root N uptake
294 and N assimilation seemed to be the key targets of the negative effect of high CO_2 on plant N
295 content (Bloom et al., 2010; Cassan et al., 2023), but these results suggest that remobilization
296 of N may also be involved. We also identified the *CA1* gene, coding for a carbonic anhydrase,
297 in the vicinity of a QTL associated with C variation under high CO_2. *CA1* is involved in the
298 regulation of stomatal opening by elevated CO_2 (Hu et al., 2015), and the β carbonic anhydrase
299 family of which *CA1* belongs is involved in the regulation of photosynthetic efficiency,
300 although *CA1* shows no significant effect under standard conditions (Sharma et al.). It would
301 be therefore interesting to assess the role of *CA1* natural genetic variation under elevated CO_2.
302 If *CA1* regulates the C variation of the ionome under elevated CO_2, this could, according to our
303 observations, significantly influence the global mineral composition of plants. Interestingly,
304 the genes identified by GWA mapping in the ionome response to high CO_2, including those
305 mentioned above, showed substantial variation at the gene expression level. We ended this
306 study with the functional validation of an association peak identified by GWA mapping for the
307 relative change of Zn content between ambient and elevated CO_2. Zn is an essential element
308 for a large number of metabolic processes in humans, and Zn deficiency, found in up to one
309 third of the world's population, leads to severe health problems. We demonstrated that *TIP2;2*
310 gene expression varied in a haplotype-specific manner, in both ambient and elevated CO_2. In

311 parallel to this, we show that loss of *TIP2;2* expression using a knock-out mutant can abolish
312 the Zn decrease observed under high CO_2. It therefore seems that variation in *TIP* expression
313 is associated with the effect that atmospheric CO_2 can have on zinc levels. A recent study
314 demonstrated that TIP2;2 was responsible for Zn retention in the roots (Wang et al., 2022). It
315 therefore seems consistent that natural accessions with the lowest expression levels of this
316 gene are those with the highest Zn content in aerial parts, due to low retention in their roots.
317 This example illustrates the potential of the resource we have generated here towards the
318 identification of genes involved in the variation of leaf ionome in response to rising CO_2, and
319 towards the characterization of the associated mechanisms. The understanding of these
320 mechanisms represents a considerable challenge in view of the current rise in atmospheric
321 CO_2, which might be useful to the coming breeding programs for crops adapted to a
322 forthcoming CO_2-rich atmosphere (Shahzad and Rouached, 2022). It must however be recalled
323 that leaf ionome is not always correlated with seed ionome, in particular in *Arabidopsis*
324 *thaliana* accessions (Campos et al., 2021). Therefore, the effect of elevated CO_2 on seed
325 ionome, certainly in major crops, must be the next target to analyze in order to pave the way
326 for the development of nutritious crops adapted to elevated CO_2.
327
328 **Methods**
329 *Data and code availability*
330 Data and R notebooks containing the analyses performed in this article can be found at
331 https://src.koda.cnrs.fr/groups/ipsim/sirene-team. RNA-seq data generated for this study are
332 available at https://www.ebi.ac.uk/biostudies/arrayexpress/studies using the accession no E-
333 MTAB-13661.
334 *Plant Material*

335 A subset of the REGMAP panel, the LANGUEDOC panel and the TOU-A panel were used in this
336 study. These populations were previously described here (Horton et al., 2012; Brachi et al.,
337 2013; Frachon et al., 2017). These populations were grown on Jiffy-7 peat pellets (Jiffy
338 Products International, NL) under ambient (~420 ppm) or elevated (900 ppm) CO_2 in the
339 growth chambers of the Microcosms experimental platform at the Montpellier European
340 Ecotron CNRS. Five replicates of each accession were randomly distributed in the growth
341 chambers. The concentration of 900 ppm of CO_2 was chosen as current CO_2 emissions align
342 with the IPCC's RCP8.5 model, which predicts a CO2 concentration of around 900 ppm in 2100.
343 Growth conditions were 6-h/22-h light (22°C) / dark (20°) photoperiod, with 200 µmol m^{-2} s^{-1}
344 light intensity and 65% of hygrometry. Plants were watered twice a week with a growth
345 solution containing KH_2PO_4 1 mM, $MgSO_4$ 1 mM, K_2SO_4 250 µM, $CaCl_2$ 250 µM, Na-Fe-EDTA
346 100 µM, KNO_3 10 mM, KCl 50 µM, H_3BO_3 30 µM, $MnSO_4$ 5 µM, $ZnSO_4$ 1 µM, $CuSO_4$ 1 µM,
347 $(NH_4)_6Mo_70_{24}$ 0,1 µM, as described by (Gansel et al., 2001). The entire rosettes were collected
348 three weeks after sowing. The *tip2;2-1* mutant line corresponds to the *SALK_152463* allele
349 (Wang et al., 2022).

350 *Ionome analysis*

351 From 3 to 5 replicates per accession were pooled and used for each ionome analysis. Total C
352 and N content was obtained from dried shoot tissue using an Elementar Pyrocube analyzer.
353 Cu, Fe, Mg, Mn, Na and Zn content was obtained from dry shoot tissue mixed with 750 µl of
354 nitric acid (65% [v/v]) and 250 µl of hydrogen peroxide (30% [v/v]). After one night at room
355 temperature, samples were mineralized at 85°C during 24 hours. Once mineralized, 4 ml of
356 milliQ water was added to each sample. Mineral contents present in the samples were then
357 measured by microwave plasma atomic emission spectroscopy (MP-AES, Agilent
358 Technologies).

359 *Removal of outlier observations*

360 Prior to GWAS and multivariate analyses such as PCA or clustering, mineral composition
361 measures were pre-processed to remove technical outliers. For a given element and CO_2
362 condition, the values positioned more than 5 median absolute deviations away from the
363 median were removed from the dataset. The number of outliers removed from each dataset
364 is indicated in Supplemental Table 7.

365 *PCA and Clustering*

366 Principal Component Analysis was performed using the R *ade4* package after the prior scaling
367 of the variables to a z-score. Clustering of the REGMAP panel based on the relative changes of
368 the mineral composition of each accession has been done using a k-means clustering with the
369 R *kmeans* function. For this step, the variables were also scaled to a z-score. The number of
370 clusters in the k-means algorithm was chosen by the elbow method on the criteria of cluster
371 homogeneity (within-sum of squares).

372 *GWAs*

373 Genome-Wide Association mapping was performed using the R *statgenGWAs* package.
374 Genotype data was prepared using the *codeMarkers* function, removing duplicated SNPs and
375 filtering for a minimum allele relative frequency of 0.04. Associations were performed by the
376 *runSingleTraitGwas* function, that implements the EMMA algorithm. Population structure was
377 modeled via a kinship matrix built from the Astle method. Manhattan plots were drawn using
378 the *manPlotFast* function of the *ramwas* R package.

379 *RNA-seq experiments*

380 Plants from the Columbia accession were grown in hydroponics to have access to the roots in
381 addition to the shoot, as previously described in (Cassan et al., 2023). Shoot or root from 5
382 plants were pooled into one biological replicate, flash frozen in liquid nitrogen, and stored at

383 -80◦C. RNA of three biological replicates were extracted from shoot or root tissues using
384 Direct-zol RNA Miniprep (Zymo Research, CA, USA), according to the manufacturer
385 recommendations. RNA-sequencing libraries were done from shoot or root total RNA using
386 standard RNA-Seq protocol method (Poly-A selection for mRNA species) by the Novogene
387 company. RNA-sequencing was performed using Illumina technology on a NovaSeq6000
388 system providing PE150 reads. The quality control and adapter trimming of raw paired-end
389 fastq files was done with *fastp* and its default parameters. Mapping to the TAIR10 reference
390 genome was performed with STAR, and using the following options:
391 --outSAMtype BAM SortedByCoordinate
392 --outFilterMismatchNmax 1
393 --outFilterMismatchNoverLmax 0.15
394 --alignIntronMin 30
395 --alignIntronMax 5000
396 Quantification of the bam files against the TAIR10 GFF3 annotation file was done using *htseq-*
397 count with options:
398 -f bam --type gene -r pos
399 --idattr=Name --stranded=no
400 Normalization and differential expression were performed using *DIANE* R package (Cassan et
401 al., 2021), with no fold change constraint, and an adjusted p-value threshold (FDR) of 0.05.
402 Lowly expressed genes with an average value across conditions under 25 reads were excluded
403 from the analysis.
404 *Quantitative real-time PCR*
405 Plants were grown in hydroponics to have access to the roots, as previously described in
406 (Cassan et al., 2023). Root tissue from 5 plants were pooled into one biological replicate, flash

407 frozen in liquid nitrogen, and stored at -80◦C. RNA were extracted from shoot or root tissues
408 using TRIZOL (Invitrogen, USA), according to the manufacturer recommendations, and DNAse
409 treated using RQ1 (Promega, USA). Reverse transcription was achieved from 1 μg of total RNA
410 with M-MLV reverse transcriptase (RNase H minus, Point Mutant, Promega, USA) using an
411 anchored oligo(dT)20 primer. Accumulation of transcripts was measured by qRT-PCR
412 (LightCycler 480, Roche Diagnostics, USA) using the SYBR Premix Ex TaqTM (TaKaRa, Japan).
413 Gene expression was normalized using *UBQ10* and *ACT2* as internal standards. Results are
414 presented as the expression relative to *UBQ10*. Sequences of primers used in RT-qPCR for
415 gene expression analysis are listed in Supplemental Table 6.
416

417 **Acknowledgments**

418 This work was supported by the I-Site Montpellier Université d'Excellence (MUSE; project
419 ECO2THREATS), the CNRS through the Mission for Transversal and Interdisciplinary Initiatives
420 (MITI) 80 PRIME program, and the Plant Biology and Breeding department of INRAE. O.C. was
421 recipient of a PhD fellowship from the CNRS. T.M. was recipient of a PhD fellowship from
422 INRAE and Région Occitanie. We thank Jiping Liu from Cornell University for the gift of *tip2;2-*
423 *1* mutant line. This study benefited from the CNRS human and technical resources allocated
424 to the Ecotron Research Infrastructure and from the state allocation "Investissement
425 d'Avenir" AnaEE France ANR-11-INBS-0001. A CC-BY public copyright license has been applied
426 by the authors to the present document.
427

428 **References**

429

430 **Ainsworth, E.A., and Long, S.P.** (2005). What have we learned from 15 years of free-air CO_2
431 enrichment (FACE)? A meta-analytic review of the responses of photosynthesis,
432 canopy properties and plant production to rising CO_2. New Phytol **165,** 351-371.

433 **Arouisse, B., Korte, A., van Eeuwijk, F., and Kruijer, W.** (2020). Imputation of 3 million SNPs
434 in the Arabidopsis regional mapping population. The Plant Journal **102,** 872-882.

435 **Balk, J., and Schaedler, T.A.** (2014). Iron cofactor assembly in plants. Annu Rev Plant Biol **65,**
436 125-153.

437 **Baxter, I., Brazelton, J.N., Yu, D., Huang, Y.S., Lahner, B., Yakubova, E., Li, Y., Bergelson, J.,**
438 **Borevitz, J.O., Nordborg, M., Vitek, O., and Salt, D.E.** (2010). A Coastal Cline in Sodium
439 Accumulation in *Arabidopsis thaliana* Is Driven by Natural Variation of the Sodium
440 Transporter AtHKT1;1. PLOS Genetics **6,** e1001193.

441 **Bloom, A.J., Burger, M., Rubio Asensio, J.S., and Cousins, A.B.** (2010). Carbon dioxide
442 enrichment inhibits nitrate assimilation in wheat and Arabidopsis. Science **328,** 899-
443 903.

444 **Bohner, A., Kojima, S., Hajirezaei, M., Melzer, M., and von Wirén, N.** (2015). Urea
445 retranslocation from senescing Arabidopsis leaves is promoted by DUR3-mediated
446 urea retrieval from leaf apoplast. The Plant Journal **81,** 377-387.

447 **Bouain, N., Cho, H., Sandhu, J., Tuiwong, P., Prom, U.T.C., Zheng, L., Shahzad, Z., and**
448 **Rouached, H.** (2022). Plant growth stimulation by high CO_2 depends on phosphorus
449 homeostasis in chloroplasts. Curr Biol.

450 **Brachi, B., Villoutreix, R., Faure, N., Hautekèete, N., Piquot, Y., Pauwels, M., Roby, D.,**
451 **Cuguen, J., Bergelson, J., and Roux, F.** (2013). Investigation of the geographical scale

452 of adaptive phenological variation and its underlying genetics in *Arabidopsis thaliana*.
453 Molecular Ecology **22,** 4222-4240.
454 **Brun, A., Smokvarska, M., Wei, L., Chay, S., Curie, C., and Mari, S.** (2022). MCO1 and MCO3,
455 two putative ascorbate oxidases with ferroxidase activity, new candidates for the
456 regulation of apoplastic iron excess in Arabidopsis. Plant Direct **6,** e463.
457 **Campos, A., van Dijk, W.F.A., Ramakrishna, P., Giles, T., Korte, P., Douglas, A., Smith, P., and**
458 **Salt, D.E.** (2021). 1,135 ionomes reveal the global pattern of leaf and seed mineral
459 nutrient and trace element diversity in *Arabidopsis thaliana*. Plant J **106,** 536-554.
460 **Cassan, O., Lebre, S., and Martin, A.** (2021). Inferring and analyzing gene regulatory networks
461 from multi-factorial expression data: a complete and interactive suite. BMC Genomics
462 **22,** 387.
463 **Cassan, O., Pimpare, L.L., Dubos, C., Gojon, A., Bach, L., Lebre, S., and Martin, A.** (2023). A
464 gene regulatory network in Arabidopsis roots reveals features and regulators of the
465 plant response to elevated CO(2). New Phytol **239,** 992-1004.
466 **Cortés, A.J., and López-Hernández, F.** (2021). Harnessing Crop Wild Diversity for Climate
467 Change Adaptation. Genes **12,** 783.
468 **Dusenge, M.E., Duarte, A.G., and Way, D.A.** (2019). Plant carbon metabolism and climate
469 change: elevated CO2 and temperature impacts on photosynthesis, photorespiration
470 and respiration. New Phytol **221,** 32-49.
471 **Ebi, K.L., and Loladze, I.** (2019). Elevated atmospheric CO(2) concentrations and climate
472 change will affect our food's quality and quantity. Lancet Planet Health **3,** e283-e284.
473 **Frachon, L., Libourel, C., Villoutreix, R., Carrere, S., Glorieux, C., Huard-Chauveau, C.,**
474 **Navascues, M., Gay, L., Vitalis, R., Baron, E., Amsellem, L., Bouchez, O., Vidal, M., Le**
475 **Corre, V., Roby, D., Bergelson, J., and Roux, F.** (2017). Intermediate degrees of

476 synergistic pleiotropy drive adaptive evolution in ecological time. Nat Ecol Evol **1,** 1551-
477 1561.
478 **Gansel, X., Munos, S., Tillard, P., and Gojon, A.** (2001). Differential regulation of the NO_3^- and
479 NH4+ transporter genes *AtNrt2.1* and *AtAmt1.1* in Arabidopsis: relation with long-
480 distance and local controls by N status of the plant. Plant J **26,** 143-155.
481 **Gao, Y., de Bang, T.C., and Schjoerring, J.K.** (2019). Cisgenic overexpression of cytosolic
482 glutamine synthetase improves nitrogen utilization efficiency in barley and prevents
483 grain protein decline under elevated CO_2. Plant Biotechnology Journal **17,** 1209-1221.
484 **Gaufichon, L., Marmagne, A., Belcram, K., Yoneyama, T., Sakakibara, Y., Hase, T., Grandjean,**
485 **O., Clément, G., Citerne, S., Boutet-Mercey, S., Masclaux-Daubresse, C., Chardon, F.,**
486 **Soulay, F., Xu, X., Trassaert, M., Shakiebaei, M., Najihi, A., and Suzuki, A.** (2017).
487 ASN1-encoded asparagine synthetase in floral organs contributes to nitrogen filling in
488 Arabidopsis seeds. The Plant Journal **91,** 371-393.
489 **Gojon, A., Cassan, O., Bach, L., Lejay, L., and Martin, A.** (2023). The decline of plant mineral
490 nutrition under rising CO_2: physiological and molecular aspects of a bad deal. Trends
491 in Plant Science **28,** 185-198.
492 **Horton, M.W., Hancock, A.M., Huang, Y.S., Toomajian, C., Atwell, S., Auton, A., Muliyati,**
493 **N.W., Platt, A., Sperone, F.G., Vilhjálmsson, B.J., Nordborg, M., Borevitz, J.O., and**
494 **Bergelson, J.** (2012). Genome-wide patterns of genetic variation in worldwide
495 Arabidopsis thaliana accessions from the RegMap panel. Nature Genetics **44,** 212-216.
496 **Hu, H., Rappel, W.-J., Occhipinti, R., Ries, A., Böhmer, M., You, L., Xiao, C., Engineer, C.B.,**
497 **Boron, W.F., and Schroeder, J.I.** (2015). Distinct Cellular Locations of Carbonic
498 Anhydrases Mediate Carbon Dioxide Control of Stomatal Movements Plant Physiology
499 **169,** 1168-1178.

500 **Huard-Chauveau, C., Perchepied, L., Debieu, M., Rivas, S., Kroj, T., Kars, I., Bergelson, J.,**
501 **Roux, F., and Roby, D.** (2013). An atypical kinase under balancing selection confers
502 broad-spectrum disease resistance in Arabidopsis. PLoS Genet **9,** e1003766.
503 **Kim, S., Plagnol, V., Hu, T.T., Toomajian, C., Clark, R.M., Ossowski, S., Ecker, J.R., Weigel, D.,**
504 **and Nordborg, M.** (2007). Recombination and linkage disequilibrium in *Arabidopsis*
505 *thaliana*. Nature Genetics **39,** 1151-1155.
506 **Lam, H.-M., Wong, P., Chan, H.-K., Yam, K.-M., Chen, L., Chow, C.-M., and Coruzzi, G.M.**
507 (2003). Overexpression of the *ASN1* Gene Enhances Nitrogen Status in Seeds of
508 Arabidopsis. Plant Physiology **132,** 926-935.
509 **Lee, S., Ricachenevsky, F.K., and Punshon, T.** (2021). Functional overlap of two major
510 facilitator superfamily transporter, ZIF1, and ZIFL1 in zinc and iron homeostasis.
511 Biochemical and biophysical research communications **560,** 7-13.
512 **Loladze, I.** (2014). Hidden shift of the ionome of plants exposed to elevated CO(2)depletes
513 minerals at the base of human nutrition. Elife **3,** e02245.
514 **Luthi, D., Le Floch, M., Bereiter, B., Blunier, T., Barnola, J.M., Siegenthaler, U., Raynaud, D.,**
515 **Jouzel, J., Fischer, H., Kawamura, K., and Stocker, T.F.** (2008). High-resolution carbon
516 dioxide concentration record 650,000-800,000 years before present. Nature **453,** 379-
517 382.
518 **Marcos-Barbero, E.L., Pérez, P., Martínez-Carrasco, R., Arellano, J.B., and Morcuende, R.**
519 (2021). Screening for Higher Grain Yield and Biomass among Sixty Bread Wheat
520 Genotypes Grown under Elevated CO_2 and High-Temperature Conditions. Plants **10,**
521 1596.

522 **Medek, D.E., Schwartz, J., and Myers, S.S.** (2017). Estimated Effects of Future Atmospheric
523 CO_2 Concentrations on Protein Intake and the Risk of Protein Deficiency by Country
524 and Region. Environ Health Perspect **125,** 087002.
525 **Myers, S.S., Zanobetti, A., Kloog, I., Huybers, P., Leakey, A.D., Bloom, A.J., Carlisle, E.,**
526 **Dietterich, L.H., Fitzgerald, G., Hasegawa, T., Holbrook, N.M., Nelson, R.L., Ottman,**
527 **M.J., Raboy, V., Sakai, H., Sartor, K.A., Schwartz, J., Seneweera, S., Tausz, M., and**
528 **Usui, Y.** (2014). Increasing CO_2 threatens human nutrition. Nature **510,** 139-142.
529 **North, K.A., Ehlting, B., Koprivova, A., Rennenberg, H., and Kopriva, S.** (2009). Natural
530 variation in Arabidopsis adaptation to growth at low nitrogen conditions. Plant
531 Physiology and Biochemistry **47,** 912-918.
532 **Pauls, S.U., Nowak, C., Balint, M., and Pfenninger, M.** (2013). The impact of global climate
533 change on genetic diversity within populations and species. Mol Ecol **22,** 925-946.
534 **Pearson, P.N., and Palmer, M.R.** (2000). Atmospheric carbon dioxide concentrations over the
535 past 60 million years. Nature **406,** 695-699.
536 **Roux, F., and Frachon, L.** (2022). A Genome-Wide Association study in *Arabidopsis thaliana* to
537 decipher the adaptive genetics of quantitative disease resistance in a native
538 heterogeneous environment. PLoS One **17,** e0274561.
539 **Shahzad, Z., and Rouached, H.** (2022). Protecting plant nutrition from the effects of climate
540 change. Curr Biol **32,** R725-R727.
541 **Sharma, N., Froehlich, J.E., Rillema, R., Raba, D.A., Chambers, T., Kerfeld, C.A., Kramer, D.M.,**
542 **Walker, B., and Brandizzi, F.** (2023). Arabidopsis stromal carbonic anhydrases exhibit
543 non-overlapping roles in photosynthetic efficiency and development. Plant J 2023 **115,**
544 386-397.

545 **Sun, P., Isner, J.C., Coupel-Ledru, A., Zhang, Q., Pridgeon, A.J., He, Y., Menguer, P.K., Miller,**
546 **A.J., Sanders, D., McGrath, S.P., Noothong, F., Liang, Y.K., and Hetherington, A.M.**
547 (2022). Countering elevated CO_2 induced Fe and Zn reduction in Arabidopsis seeds.
548 New Phytol **235,** 1796-1806.
549 **Tausz-Posch, S., Tausz, M., and Bourgault, M.** (2020). Elevated [CO_2] effects on crops:
550 Advances in understanding acclimation, nitrogen dynamics and interactions with
551 drought and other organisms. Plant Biol (Stuttg) **22 Suppl 1,** 38-51.
552 **Thompson, M., Gamage, D., Hirotsu, N., Martin, A., and Seneweera, S.** (2017). Effects of
553 Elevated Carbon Dioxide on Photosynthesis and Carbon Partitioning: A Perspective on
554 Root Sugar Sensing and Hormonal Crosstalk. Front Physiol **8,** 578.
555 **Umnajkitikorn, K., Sade, N., Rubio Wilhelmi, M.D.M., Gilbert, M.E., and Blumwald, E.** (2020).
556 Silencing of OsCV (chloroplast vesiculation) maintained photorespiration and N
557 assimilation in rice plants grown under elevated CO(2). Plant Cell Environ **43,** 920-933.
558 **Wang, Y., Kang, Y., Yu, W., Lyi, S.M., Choi, H.W., Xiao, E., Li, L., Klessig, D.F., and Liu, J.** (2022).
559 AtTIP2;2 facilitates resistance to zinc toxicity via promoting zinc immobilization in the
560 root and limiting root-to-shoot zinc translocation in *Arabidopsis thaliana*.
561 Ecotoxicology and Environmental Safety **233,** 113333.
562 **Yang, A., Li, Q., Chen, L., and Zhang, W.-H.** (2020). A rice small GTPase, Rab6a, is involved in
563 the regulation of grain yield and iron nutrition in response to CO_2 enrichment. Journal
564 of Experimental Botany **71,** 5680-5688.
565 **Zhu, C., Kobayashi, K., Loladze, I., Zhu, J., Jiang, Q., Xu, X., Liu, G., Seneweera, S., Ebi, K.L.,**
566 **Drewnowski, A., Fukagawa, N.K., and Ziska, L.H.** (2018). Carbon dioxide (CO_2) levels
567 this century will alter the protein, micronutrients, and vitamin content of rice grains

with potential health consequences for the poorest rice-dependent countries. Sci Adv **4,** eaaq1012.

Figure legends :

Figure 1: Elevated CO_2 negatively impacts the ionome content at the population-scale level in *Arabidopsis thaliana*. A. Representation of the experimental design used in this study. The content of eight mineral elements was assessed for around 600 *Arabidopsis thaliana* accessions coming from the REGMAP (B), LANGUEDOC (C) and TOU-A (D) populations. Each dot represents the value of the content of a mineral element for one accession (yellow: ambient CO_2 (aCO_2, ~420 ppm), blue: elevated CO_2 (eCO_2, 900 ppm). N (% of dry weight), Fe ($\mu g.g^{-1}$ dry weight), Zn ($\mu g.g^{-1}$ dry weight), Cu ($\mu g.g^{-1}$ dry weight), Mg ($\mu g.g^{-1}$ dry weight), Mn ($\mu g.g^{-1}$ dry weight), Na ($\mu g.g^{-1}$ dry weight), C (% of dry weight). Asterisks indicate significant differences (Paired Wilcoxson test; *, $P < 0.05$; **, $P < 0.005$; ***, $P < 0.0005$). ns; not significant.

Figure 2: Elevated CO_2 leads to high phenotypic diversity of ionome response in *Arabidopsis thaliana.* Distributions of the relative change (%) of the content of 8 mineral elements between elevated CO_2 and ambient CO_2, in each population (A: REGMAP, B: LANGUEDOC, C: TOU-A). Each dot represents the value of the relative change of the content a mineral element for one accession. The name of the element appears in bold if the mean of the element in elevated CO_2 is significantly different from the mean of the element in ambient CO_2 (Paired wilcoxon test, significance threshold of 0.05).

Figure 3: Elevated CO_2 results in a general pattern of ionome variation common to most accessions constituting natural populations of *Arabidopsis thaliana.* Principal Component Analysis (PCA) was performed using the variation of each element in response to elevated CO_2.

A. Natural accessions were positioned on the PCA and colored based on population. B. Contribution of each element to the PCA axis.

Figure 4: Variation in the response of the ionome to elevated CO_2 identifies contrasting subpopulations inside the REGMAP panel. K-means clustering was performed in the REGMAP accessions to identify different subpopulations. Each accession is represented by a dot, connected by a line between each element. Cluster 1:65 accessions. Cluster 2: 25 accessions. Cluster 3: 69 accessions.

Figure 5: Genetic architecture of the response of the ionome to elevated CO_2 in the REGMAP panel of *Arabidopsis thaliana.* A. Manhattan plots for the content of eight mineral elements under elevated CO_2, or for the relative change of the content of mineral elements between elevated CO_2 and ambient CO_2. For each Manhattan plot, SNPs with the 50 most significant P-value, located above the horizontal line, are colored. Bar plots showing the number of SNPs identified by GWAs for traits under elevated CO_2 (B) or for the relative change of the content of mineral elements between elevated CO_2 and ambient CO_2 (C) that are unique to one element or shared between 2 or 3 traits.

Figure 6: Identification of genes detected by GWA mapping and differentially regulated by elevated CO_2. Intersection between elevated CO_2-DEG in shoot (A) or root (B) and genes identified by GWA mapping. UpSet plots display the number of elevated CO_2-DEG that are associated to a locus identified for the content or the relative change of one or several mineral elements under elevated CO_2. Illustration of the pattern of elevated CO_2-DEG in shoot (C) or root (D) also identified by GWA mapping.

Figure 7: Natural variation of the *TIP2;2* gene is associated with improved responses of Zn content to elevated CO_2. A. Manhattan plot of the relative change of Zn content between elevated CO_2 and ambient CO_2 showing the presence of a peak closed to the *TIP2;2* locus. **B.** Comparison of haplotypes and their relative change of Zn content between elevated CO_2 and ambient CO_2. Three SNPs located at the *TIP2;2* locus are associated to an improvement of Zn content under elevated CO_2 for accessions that possess them (haplotype 1) compared to the rest of the population (haplotype 0). **C, D.** Relative expression of *TIP2;2* in the roots under ambient (**C**) or elevated (**D**) CO_2 for accessions belonging to haplotype 0 or haplotype 1. Relative expression levels were calculated based on *UBQ10* as internal control. Horizontal black line represented the median of each group of haplotypes. ***P < 0,001, **P < 0,01, unpaired Mann-Whitney test. **E.** Shoot Zn content under ambient or elevated CO_2 for WT (Columbia) and *tip2;2-1* mutant. Data are presented as the mean (with SD) of 5 and 6 biological repeats for the WT and *tip2;2-1*, respectively. **P < 0.01, unpaired Mann-Whitney test.